Surface oxygen species dictate reaction pathways in platinum-catalyzed aqueous phase reforming of methanol

Yuyao Yang[a,b,1], Xuan Bie[a,b,1], Yingbo Zhu[a,b], Xuelong Quan[a,b], Bocheng Yu[a,b], Qinghai Li[a,b], Yanguo Zhang[a,b], Hui Zhou[a,b,*]

[a] *Key Laboratory for Thermal Science and Power Engineering of Ministry of Education, Beijing Key Laboratory of CO_2 Utilization and Reduction Technology, Department of Energy and Power Engineering, Tsinghua University, Beijing 100084, P.R. China*

[b] *Shanxi Research Institute for Clean Energy, Tsinghua University, Taiyuan, Shanxi 030000, P.R. China*

**Corresponding author: huizhou@tsinghua.edu.cn*

[1]These authors contributed equally to this work.

Table of contents

Supplementary figures

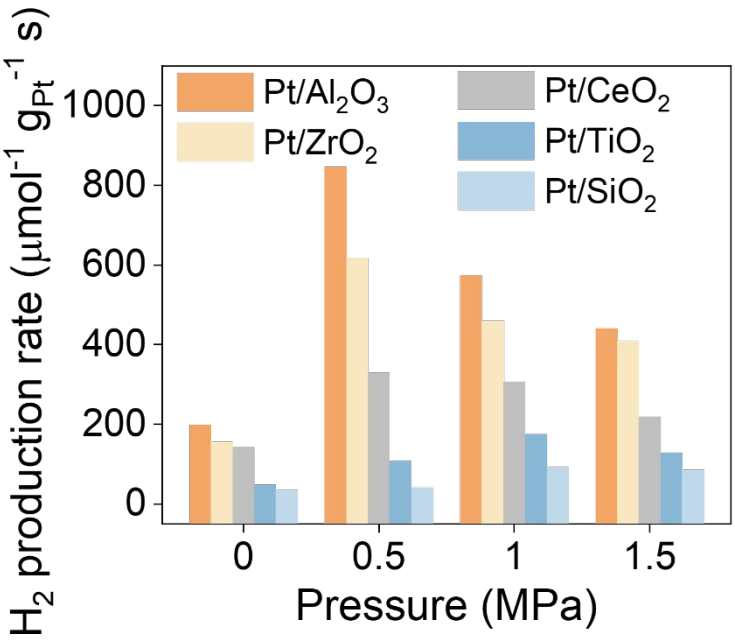

Figure S1. H_2 production rates of Pt/oxide catalysts at different pressures.

Reaction pressure also has a significant impact on APRM performance, revealing that the catalytic activity initially increases with increasing pressure and then decreases at higher pressures. This is because at low N_2 pressure, the partial pressure of gaseous products decreases, which facilitates the reaction to proceed in the forward direction. At higher N_2 pressures, the desorption of products is inhibited, resulting in a decrease in catalytic activity. Among the various pressure conditions examined, Pt/Al_2O_3 consistently exhibits the highest hydrogen production, reaching a maximum at 0.5 MPa.

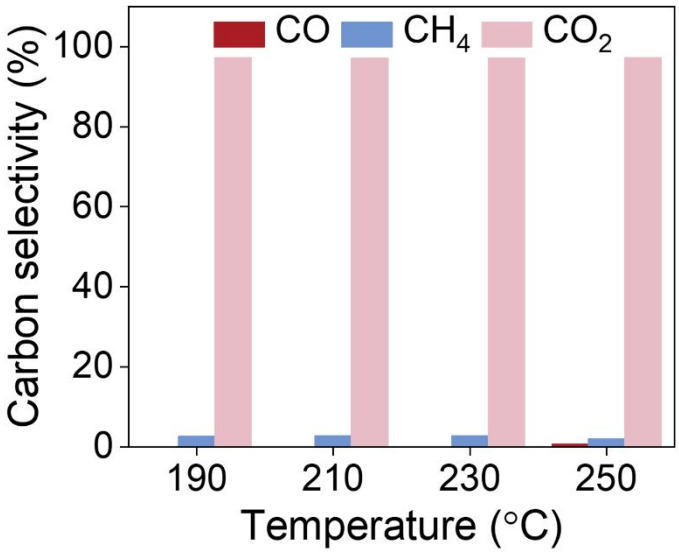

Figure S2. The carbon selectivity of APRM over Pt/Al_2O_3.

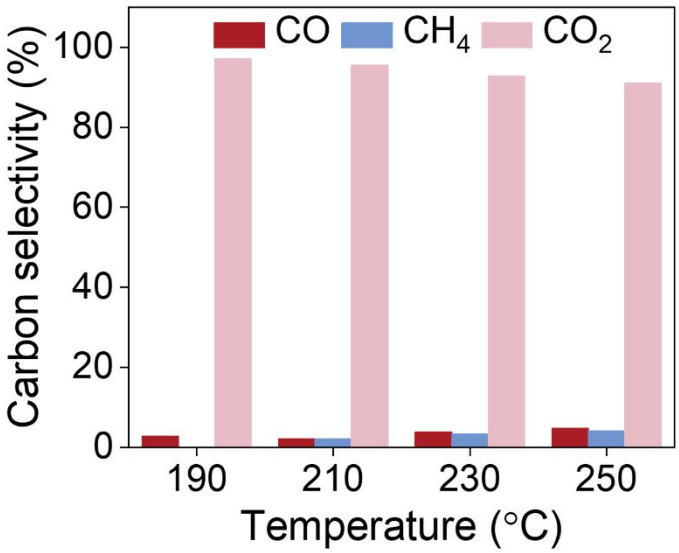

Figure S3. The carbon selectivity of APRM over Pt/ZrO_2.

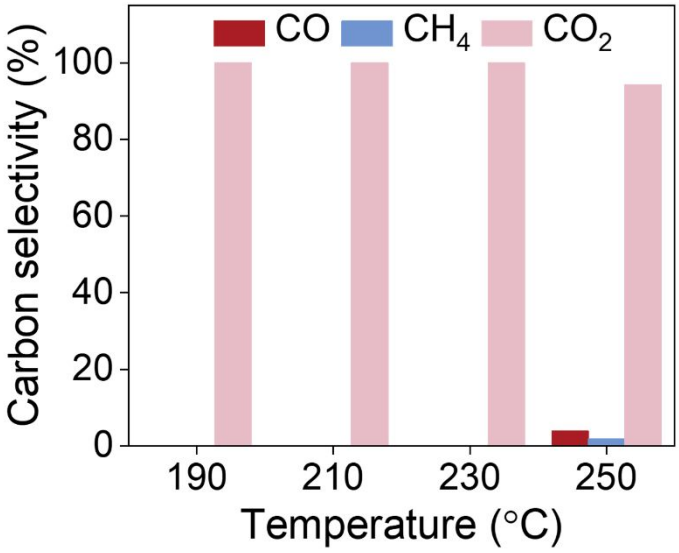

Figure S4. The carbon selectivity of APRM over Pt/CeO_2.

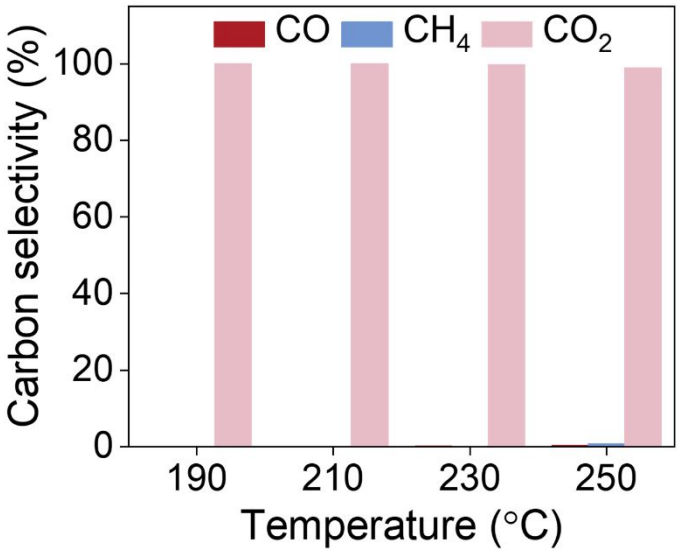

Figure S5. The carbon selectivity of APRM over Pt/TiO_2.

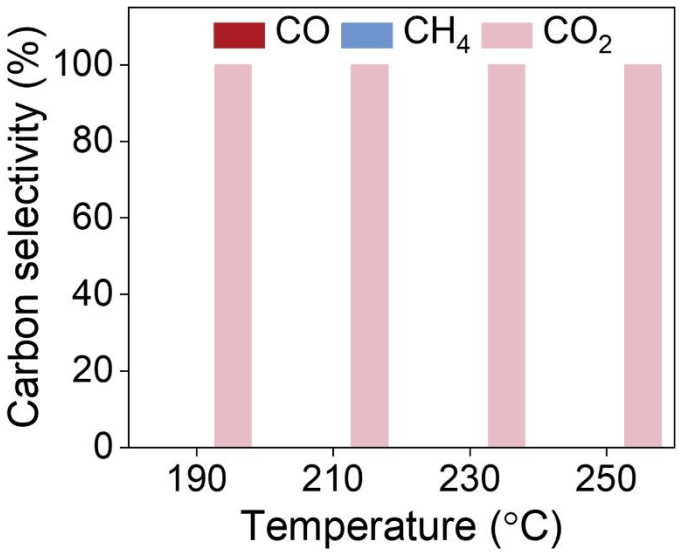

Figure S6. The carbon selectivity of APRM over Pt/SiO_2.

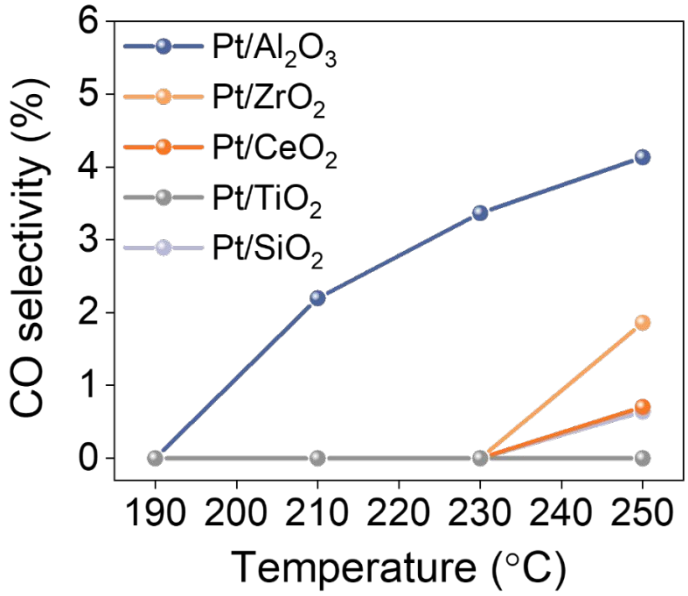

Figure S7. The CO selectivity of APRM over Pt/oxide catalysts.

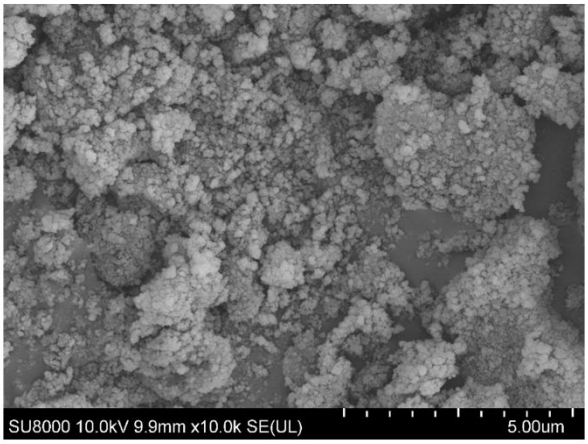

Figure S8. SEM images of Al_2O_3.

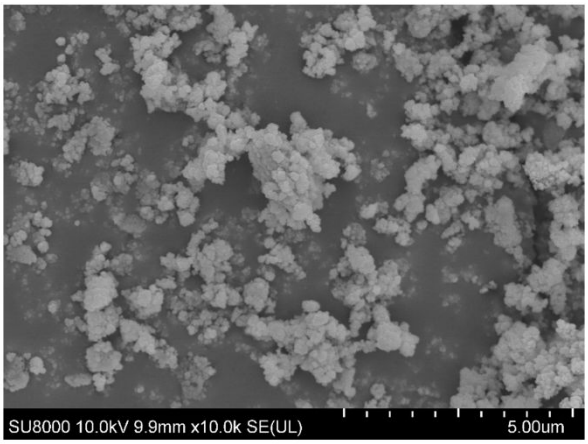

Figure S9. SEM images of ZrO_2.

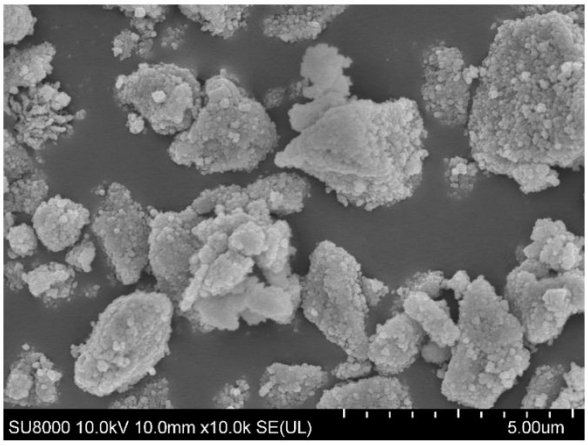

Figure S10. SEM images of CeO_2.

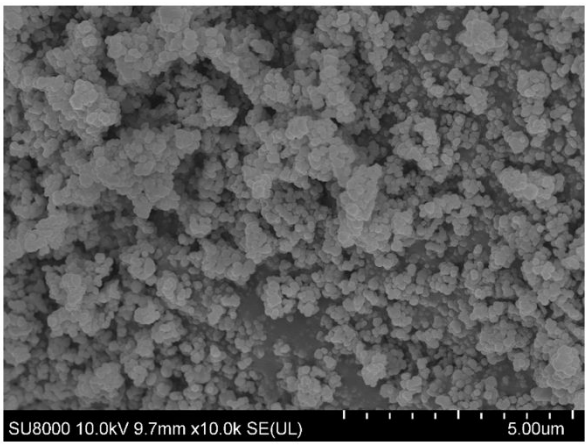

Figure S11. SEM images of TiO_2.

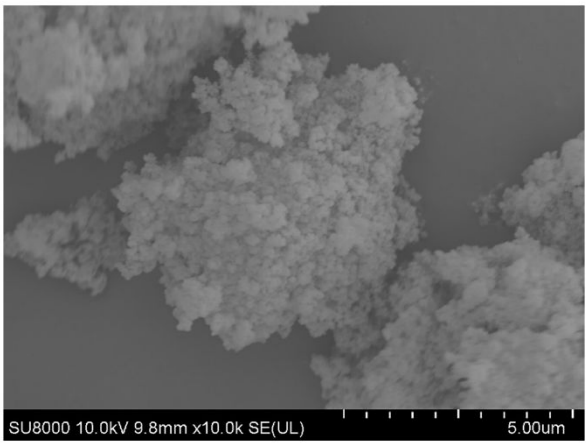

Figure S12. SEM images of SiO_2.

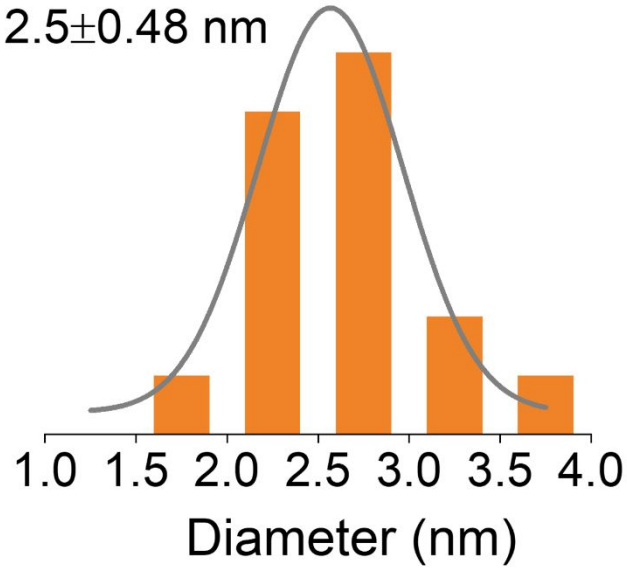

Figure S13. Pt particle size distribution on Al_2O_3.

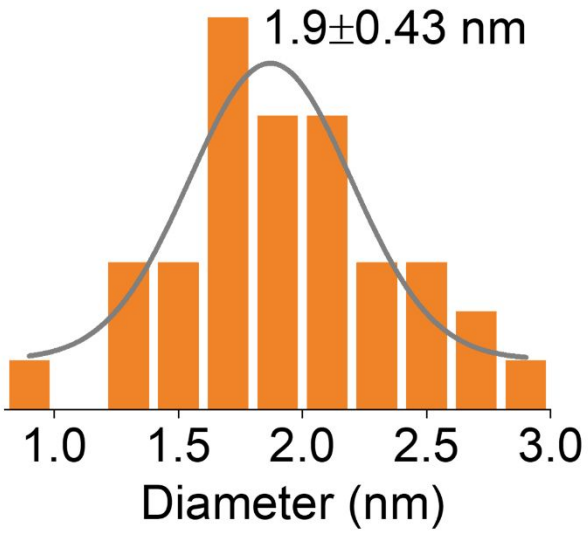

Figure S14. Pt particle size distribution on ZrO_2.

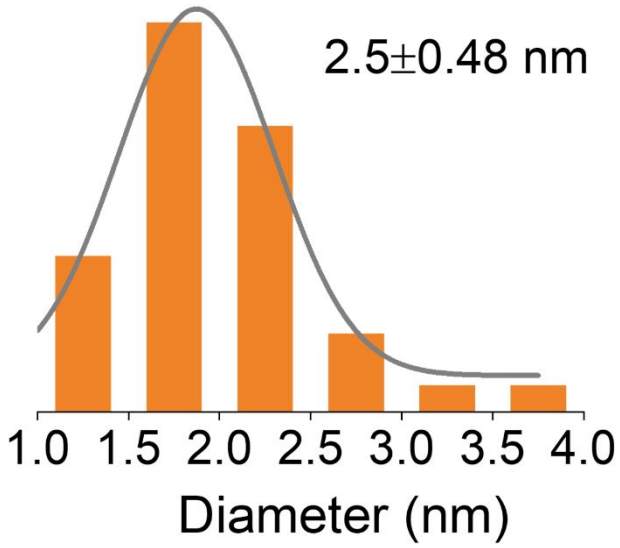

Figure S15. Pt particle size distribution on CeO_2.

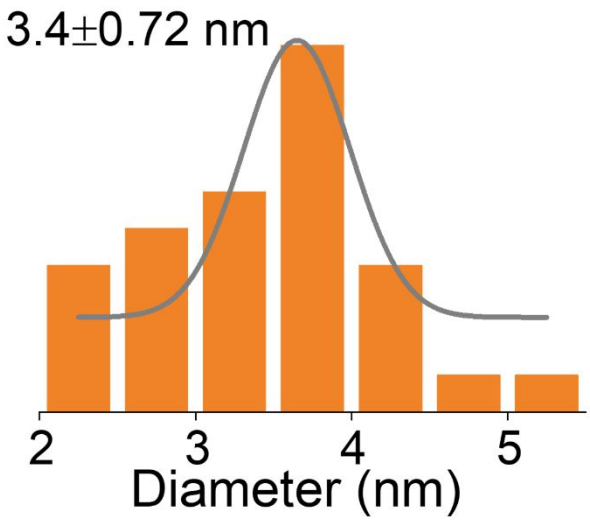

Figure S16. Pt particle size distribution on TiO_2.

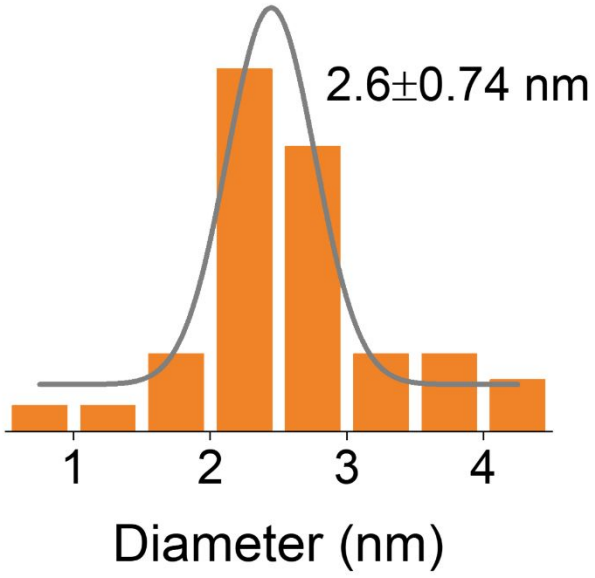

Figure S17. Pt particle size distribution on SiO_2.

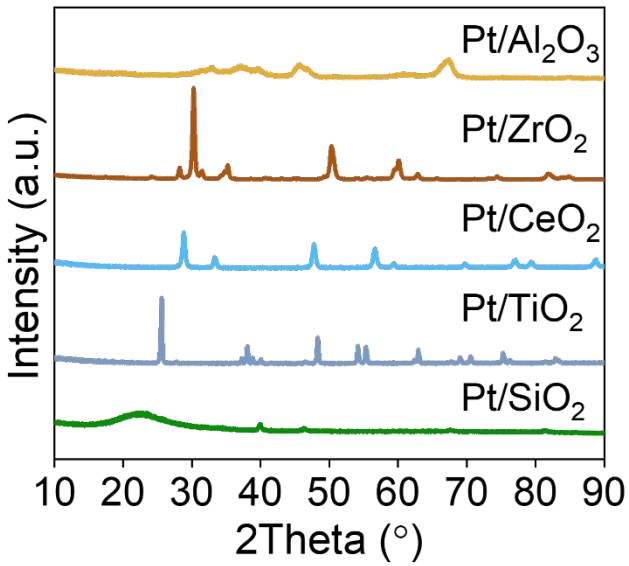

Figure S18. The XRD patterns of Pt/oxide catalysts.

Regarding crystallographic phase selection, the most catalytically active phase previously reported for each oxide was chosen. The characteristic diffraction peaks of the corresponding oxide can be observed in the XRD pattern (Fig. S18). The diffraction peaks at 2θ=31.9, 37.9, 45.7, and 66.6 ° can be indexed to the face-centered cubic Al_2O_3 phase (γ-Al_2O_3), which usually has the largest surface area and suitable acidity among various Al_2O_3[1]. These characteristics have been considered crucial for facilitating Pt dispersion and reactant adsorption in APRM[2]. Pt/ZrO_2 consists of a mixture of cubic (c-ZrO_2) and monoclinic crystal (m-ZrO_2) phases, which can provide abundant phase boundaries for interfacial interactions. The Pt/CeO_2 and Pt/TiO_2 exhibit cubic and tetragonal crystal phases, respectively, both featuring rich defective sites. The inert Pt/SiO_2 features an amorphous structure, which is typical of SiO_2 supports and serves as a reference support in APRM. Besides, the diffraction peaks of Pt are not detected in XRD, due to its uniform dispersion.

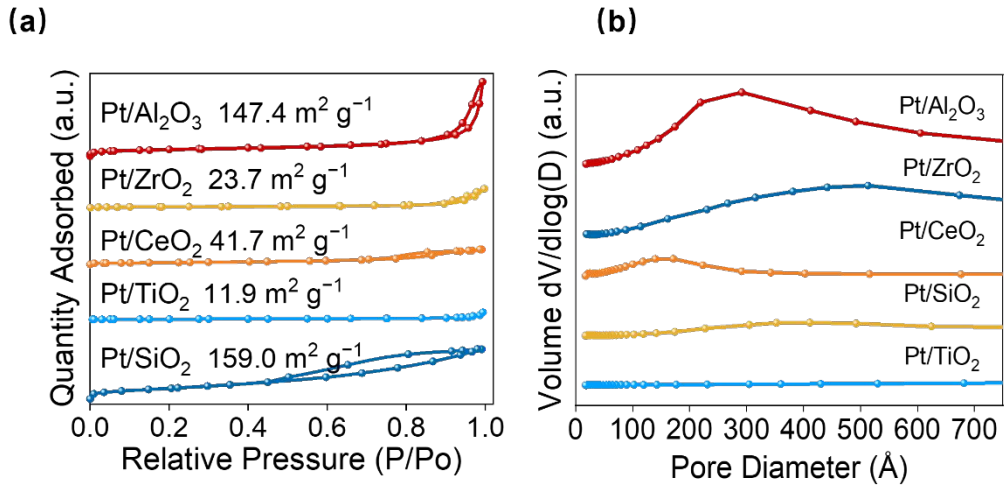

Figure S19. BET surface area analysis of catalysts. (a) Isothermal adsorption-desorption curve, (b) Pore-size distribution.

The surface areas and pore structure of these catalysts were measured by N_2 adsorption/desorption experiments (Fig. S19). The catalysts exhibit distinct BET surface areas, ranging from 11.9 to 159.0 m^2 g^{-1}, with the following order: Pt/SiO_2 > Pt/Al_2O_3 > Pt/CeO_2 > Pt/ZrO_2 > Pt/TiO_2 (Table S2). All samples display a Type IV isotherm with H3-type hysteresis loop, implying slit-shaped pores formed by the aggregation of plate-like particles. This indicates that the Pt/Al_2O_3 and Pt/SiO_2 catalysts possess larger surface areas, which can provide more anchoring sites for Pt dispersion and thus contribute to the enhanced catalytic activity of Pt/Al_2O_3. Despite the lower surface areas of Pt/TiO_2, Pt/CeO_2, and Pt/ZrO_2, the latter two still exhibit higher catalytic activity, which is attributed to their distinct oxygen species rather than surface areas (vide infra).

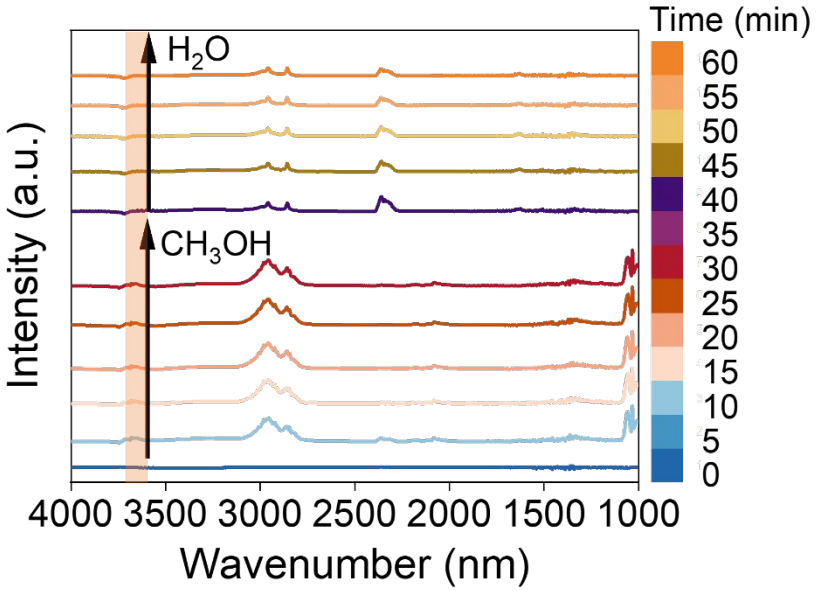

Figure S20. In-situ DRIFTS over Pt/TiO_2 catalyst upon the separate introduction of methanol and water.

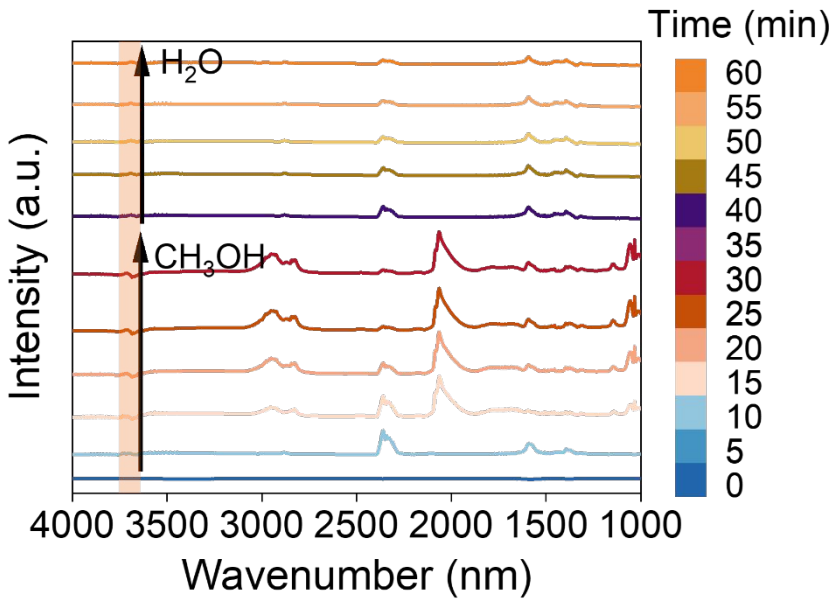

Figure S21. In-situ DRIFTS over Pt/ZrO_2 catalyst upon the separate introduction of methanol and water.

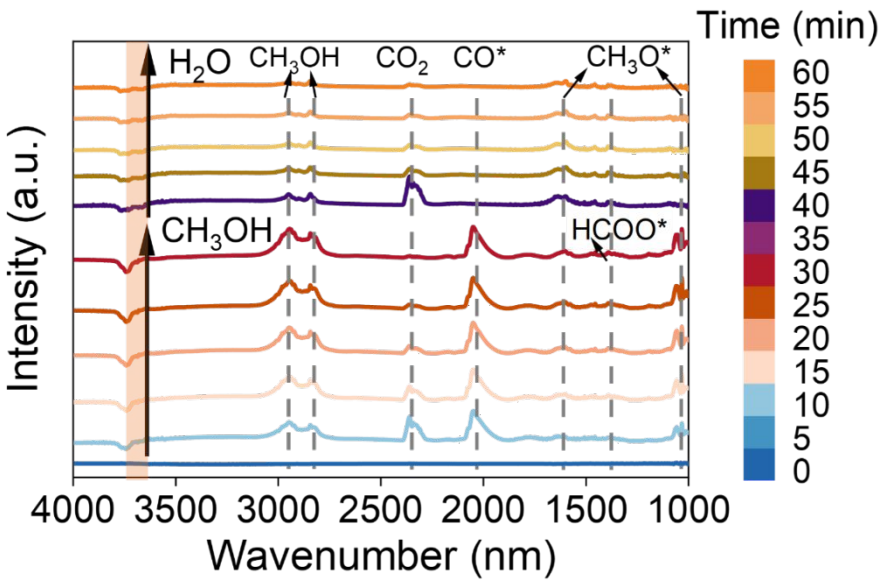

Figure S22. In-situ DRIFTS over Pt/nanorod Al_2O_3 catalyst upon the separate introduction of methanol and water.

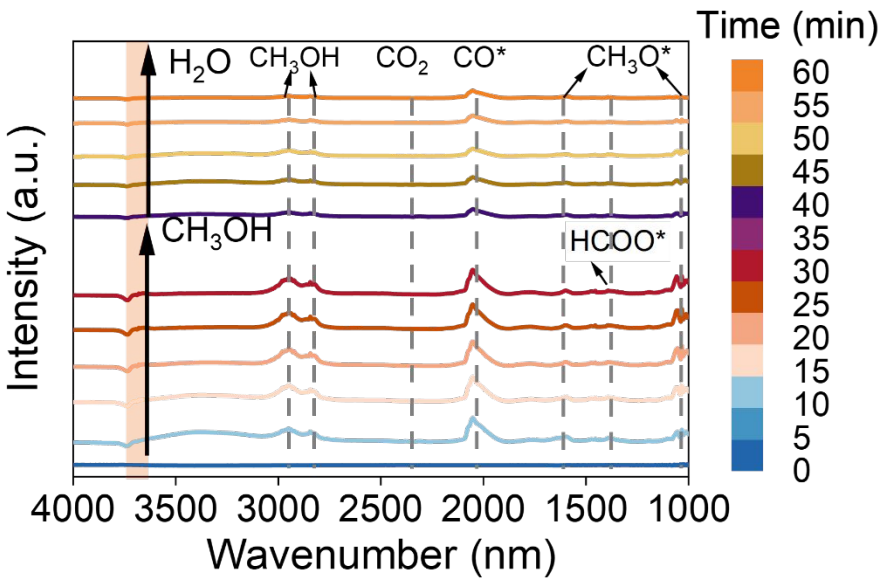

Figure S23. In-situ DRIFTS over Pt/nanosheet Al_2O_3 catalyst upon the separate introduction of methanol and water.

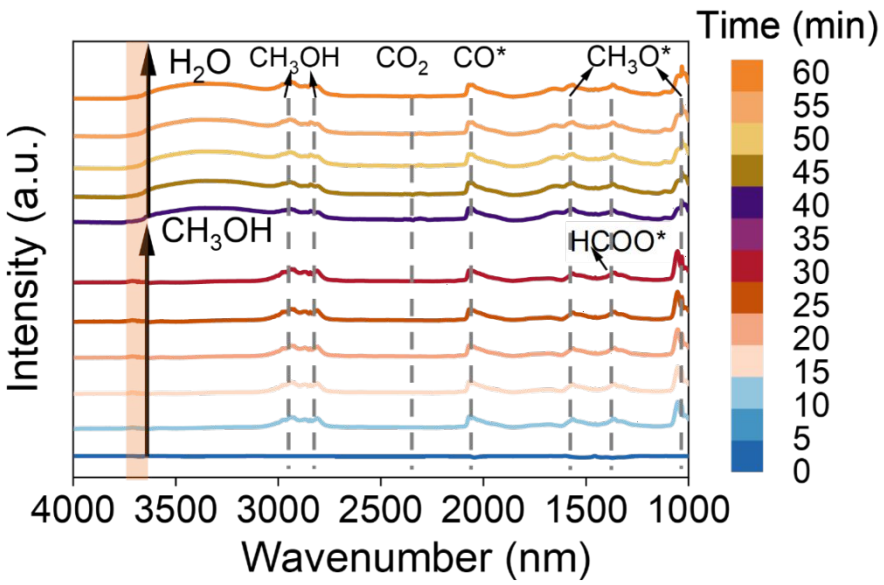

Figure S24. In-situ DRIFTS over Pt/nanorod CeO_2 catalyst upon the separate introduction of methanol and water.

Supplementary tables

Table S1. Elemental analysis of Pt/oxide catalysts

Entry	Sample	Pt loading (wt%)[a]
1	Al_2O_3	0.84
2	ZrO_2	0.93
3	CeO_2	0.81
4	TiO_2	0.91
5	SiO_2	0.85

a. Measured by ICP-OES (wt%).

Table S2. Surface area and pore characteristics of the catalysts

Sample	BET surface area ($m^2\ g^{-1}$)	Pore diameter ($cm\ g^{-1}$)	Pore size (Å)
Al_2O_3	147.4	0.72	204.0
SiO_2	159.0	0.73	238.7
ZrO_2	23.7	0.11	235.6
CeO_2	41.7	0.11	104.4
TiO_2	11.9	0.05	197.4

Table S3. XPS fitting parameters of O 1s for Pt/oxide catalysts

Sample	State	O 1s B. E. (eV)[a]	FWHM (eV)[b]	Ratio (%)
$Pt/Al2O_3$	O_L[c]	530.7	2.1	51.3
	OH[d]	532.1	2.4	48.7
Pt/ZrO_2	O_L	529.7	1.4	70.9
	O_V[e]	530.8	1.5	13.5
	OH	532.1	1.9	15.6
Pt/CeO_2	O_L	529.7	1.2	59.5
	O_V	530.8	2.2	26.2
	OH	532.1	2.4	14.3
Pt/TiO_2	O_L	529.7	1.3	61.4
	O_V	530.8	2.2	23.9
	OH	532.1	2.2	14.7
Pt/SiO_2	O_L	530.6	1.3	8.3
	OH	532.1	2.0	91.7

a. Binding energy

b. Peak width at half height

c. Lattice oxygen

d. Hydroxyl groups

e. Oxygen vacancies

Table S4. XPS fitting parameters of Pt 4f for Pt/oxide catalysts

Sample	State	Pt 4f 7/2 B. E. (eV)[a]	FWHM (eV)[b]	Ratio (%)
Pt/ZrO_2	Pt^{2+}	72.0	2.3	87.0
	Pt^{4+}	73.5	1.9	13.0
Pt/CeO_2	Pt^{2+}	72.0	1.9	81.3
	Pt^{4+}	73.5	1.6	18.7
Pt/TiO_2	Pt^0	71.1	2.2	100
Pt/SiO_2	Pt^0	70.3	1.1	100

a. Binding energy

b. Peak width at half height

References

[1] Wu Q, Zhong Y, Zhou L, Zhu M, Liu S, Qin R, et al. 2024 Oxygen vacancy-enriched alumina stabilized Pd nanocatalysts for selective hydrogenation of phenols. Journal of the American Chemical Society 146:32263-8

[2] Kwak JH, Hu J, Mei D, Yi C, Kim DH, Peden CH, et al. 2009 Coordinatively unsaturated Al3+ centers as binding sites for active catalyst phases of platinum on γ-Al2O3. Science 325:1670-3